Chapter 4

Application of Implemented Plasticity to Slope Stability Analysis

the developed Mohr-Coulomb plasticity model was first tested on simple examples to debug the code. This process provided also a good opportunity for testing the code on a practical problem. The reconstruction of the Chotek road and the local bridge started in 2004. There were doubts about the stability of the stratified rock cliff under the bridge. It was necessary to analyze the reliability of the whole slope with the very heterogeneously stratified cliff in the "letená" stratum.

The numerical analysis,commissioned by PUDIS a.s.,imposed several key requirements on the computation model:

- Analysis should be performed in several selected locations under the piers.

- These selected locations under the piers should be modeled by a 3D model based on perpendicular sections in pier axes.

- The problem should be solved by the FEM with nonlinear material behavior.

- Real geological composition of the rock strata in the necessary range for the given common slope and skew of the strata were to be used.

4.1 Description of the Situation

A slight but permanently unstable behavior of the elevated road carrying a roadway and tram tracks in both directions in the historical centre of Prague (Chotek road) and the ambient rock mass has been monitored for over twenty years. The movement values of the order of several millimetres per year have been measured. The upper part of the elevated road is founded on a heterogeneously stratified rock cliff. These phenomena resulted in the concern about the rock mass stability, particularly under the pier foundations. It was found necessary to analyze reliability and to assess the risk of the whole slope with the cliff in the very heterogeneously stratified Llandeilo stratum de1b (the flysch zone of Prague Ordovician). The significance of the task was intensified by the position of the new "Hoffihotel" closely below the cliff - see Fig. (4.1) and (4.2).

The Chotek road was built several centuries ago across a steep slope some 25 m high of a rock cliff. In the course of centuries the road was modified and reconstructed several

Figure 4.1: View of the eastern part of the cliff with the elevated road and of the hotel under the cliff. The upper part of the slope is at the upper left.

times; the same applies also to ambient buildings. The elevated road was erected at the end of the 60s (1967-1969) of last century. The last interference with the slope in this area was the construction of the Hoffihotel in 1991. At that time the last buildings below the road were demolished and a part of the slope was excavated and secured by temporary anchorage and a precast revetment wall to make room for the hotel building. At present the road carries a tramway body over 8 m wide with two tracks and a single lane carriageway of variable width on its either side. On top of the elevated highway the upward lane is about 5 m and the downward lane is about 3.5 m wide. The cut in the slope above the road is secured by a masonry wall. The subject of the investigation was the risk of the elevated road structure on a steep slope with a rock cliff. The height of the cliff is about 25 m and in addition to that the height and the slope were increased by the excavations for the basement of the Hoffihotel building. The object of the analysis was the reliability and the risk of the rock mass under the footings of the elevated road piers, possibly the reliability and risk of the slope as a whole. The rock mass is covered with thin strata of slope sediments and made-up ground of unstable state. The rock mass strata crop out of the slope under the angle of 45° - 55° with a 0° - 7° skew and show polish on strata surfaces. The rock mass consists mostly of silty-sandy schist with frequent quartzite bands (of 30-120 mm thickness, as a rule, frequently 250 mm and exceptionally as many as 400 mm - see Fig. (4.3)). The surface of the rock mass is weathered to a depth of some 3 m.

Figure 4.2: View of the excavation and temporary retaining structures of the hotel site. The elevated road is at the top.

4.2 Geological Conditions

The Chotek road is situated in Prague basin, partial sedimentation region of extensive barrandien synklinorium, the rock sub-base of which consists in a folded complex of silty-sandy slate, sandstone and quartzite of Paleozoic age. Younger geological strata in this territory are represented by a Quaternary cover. Generally, the geological conditions can be chracterized as complicated. The rock sub-base consists of letná strata (Ordovician - Beroun). According to weathering stages the letná strata can be characterized as disintegrated (highly and mildly), partly disintegrated and nondisintegrated. The rock sub-base is covered with the embankments and deluvial deposits.

In the area of interest the following strata have been found:

- anthropogenic deposits and embankment - AN - found in the topmost layers in the whole area and classified as recent sediments. The embankment consists of dug-up and displaced soil and rock from original rock base (road embankment body), but also of building materials from demolished buildings, ashes, dross, remains and others waste, which generate free voids and thereby induce also the long-term creep of this embankment.

- deluvial deposits - DEL - Pleistocene - slope soils, about 0,6 - 1,0 m thick. They are the product rock weathering and were largely generated by solifluction, i.e. by the slinking movements of partly thawed permafrost during the Ice Age.

- rock sub-base - letná strata - consisting of largely silty-sandy slate, sporadically silicated, with abundant firm quartzite inlays of 3 - 12 cm thickness as a rule , often 12 - 25 cm, rarely up to 40 cm (see Fig. (4.3)). The Letná strata (especially with regard to quartzite inlays) are very hard, considerably cohesive and, consequently, difficult disintegrate. The slope of Letná strata in the area of interest is noticeably uniform , 45° - 55° (Mach, 1958). This rock base was exposed to distinctive weathering processes. Their intensity and depth was affected by a series of factors, comparising especially the mineral composition and the petrographic character of rocks, overall geological disposition and the degree of tectonic failure and jointing of rock. The degrees of weathering can be characterized as follows :

  - disintegrated Letná strata - according to ČSN 72 1001 the degree of weathering is W4 up to W3, thickness about 1 m, density of discontinuities very high.

  - partly disintegrated Letná strata - according to ČSN 72 1001 the degree of weathering is W2, thickness about 2 m, density of discontinuities from high to very high.

  - non-disintegrated Letná strata - according to ČSN 72 1001 the degree of weathering is W1. Non-disintegrated Letná strata can be found at the depth of 3 - 9 m

Label	E[MPa]	ν	ϕ [^{o}]	c[kPa]	description
AN	30.0	0.30	30.0	5.0	Anthropogenic deposits
W1S	34.62	0.29	29.0	25.0	Slate inlay, weathering W1
W1Q	1139.65	0.14	47.5	3000.0	Quartzite inlay, weathering W1
W2S	14.054	0.30	27.0	17.5	Slate inlay, weathering W2
W2Q	507.5	0.16	44.0	1000.0	Quartzite inlay, weathering W2
W1H	1000.0	0.25	37.5	150.0	Homogenized letenské strata, weathering W1
W2H	500.0	0.28	32.5	37.5	Homogenized letenské strata, weathering W2
W3-W4	8.0	0.32	27.0	15.0	Homogenized letenské strata, weathering W3-W4
DEL	15.0	0.35	25.0	10.0	Deluvial deposits

Table 4.1: Parameters used for all geological strata

Figure 4.3: Detailed character of the Letná flysch strata with alternating schist and quartzite strata in the section under Pier No. 4.
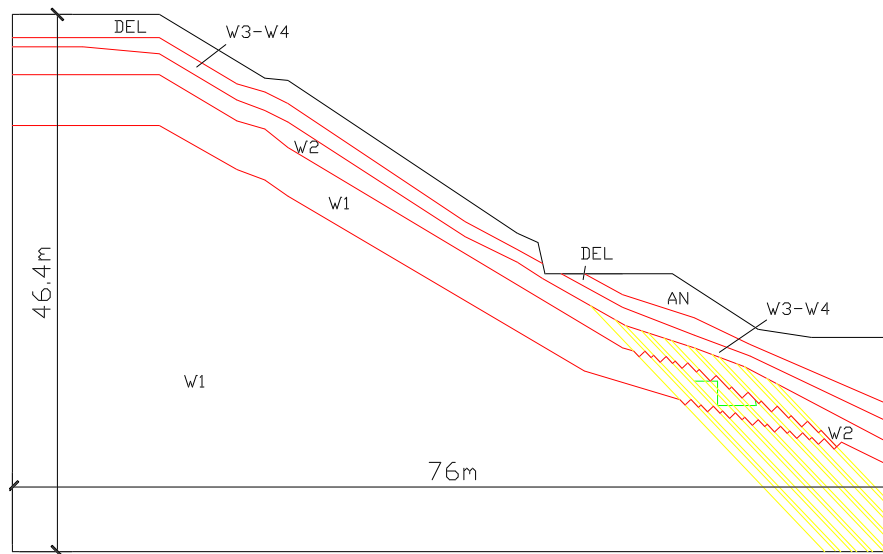

Figure 4.4: Geological situation with plotted footing base in pier No. 4. surroundings. The description of every stratum with material parameters is given in Tab. (4.1)
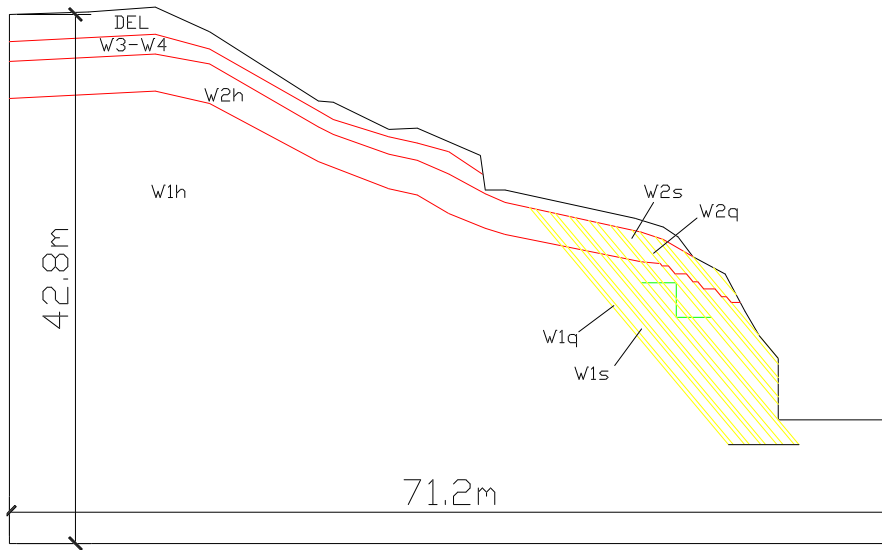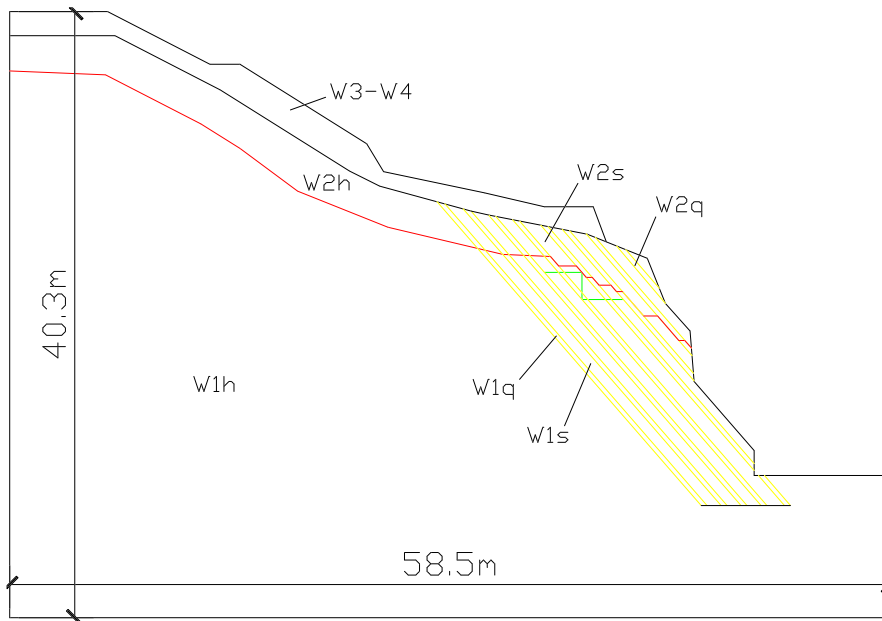
Figure 4.5: Geological situation with plotted footing base in pier No. 10. surroundings. The description of every stratum with material parameters is given in Tab. (4.1)

Figure 4.6: Geological situation with plotted footing base in pier No. 12. surroundings. The description of every stratum with material parameters is given by Tab. (4.1)

4.3 Load

Performed numerical analyses were nonlinear, therefore, the load determination proceeded according to ČSN 736203, paragraph 4a : the rock mass was loaded with the effects of the bridge and live load as a sum of standard load multiplied by relevant standard load factors. Load due to rock pressure was considered as active pressure at rest at operational values. With regard to the difficulty of calculations all load due to the bridge was reduced to the load at footing base and the bridge structure (i.e. the piers) was not simulated in calculations.

The following types of loading were taken into account :

- dead weight - consisting of the dead weight of the rock mass and the weight of the bridge, which was transformed to the load at footing base. The values of dead weight of the rock mass come from standard values of the volumetric weight of geological strata, the dead weight of the bridge was computed using geometrical basis of a 14,6 m span;

- earth pressure - rock pressure load was taken according to ČSN 736203, paragraph 15., as active pressure at rest of non-cohesive soils at operational values; however, the influence of cohesion was taken into account;

- live load - the most efficient formation of accidental load was deemed to consist of the combination of steady load by tramway transport on the filling beside the bridge - 11 kPa at the width of 8 m (paragraph 113, ČSN 736203), configuration II for load class A- 8 kPa on bridge deck in width 3 - 3.55 m, on left spaces 3.5 kPa and on sidewalk 4 kPa.
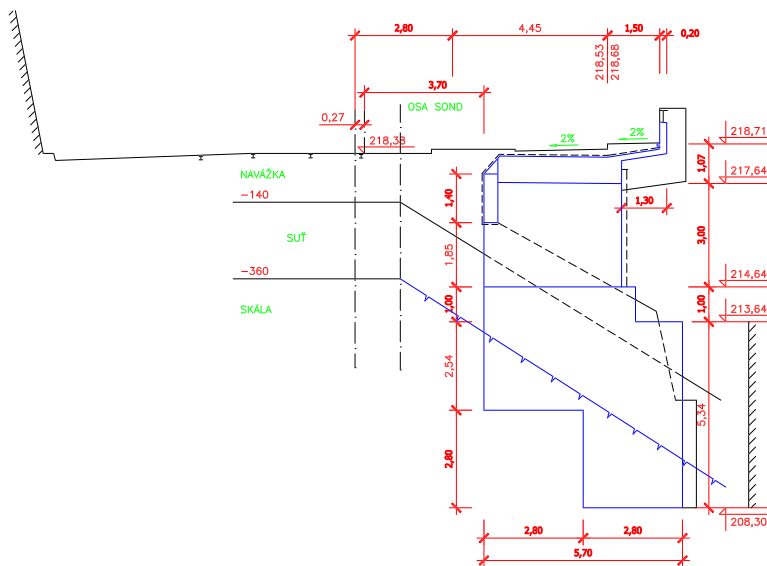

Figure 4.7: Section of pier No. 10. and of roadway

4.4 Model and Calculation

As required by the client a 3D analysis of massif segments below selected supports No. 4, 10 and 12 was performed using the Finite Element Method (FEM) with nonlinear material model. The greatest time requirements were imposed by the real strata composition including the model of their stratification in needed range. The strata slope of 49° and strata skew of 0° were used. Due to these difficulties an analysis of a 2D section on the site of pier No. 12 was made first. It showed, that the real description of stratification in a 3D model was beyond the present-day computer capacity. Therefore, adaptive techniques were applied and stratification and mesh refinement were used only in the places where the occurrence of disturbances was expected. The 3D model was based on the experiences with the 2D model. For the creation of 3D models (see Figs. (4.8) to (4.12)) a special program was developed to simplify the generation of 3D finite elements. This program generates a 3D mesh from the 2D meshed section by sequential copying the 2D segment in given steps (0.5 - 2m); at the footing base the mesh was refined as shown e.g. in Fig. (4.10). In accordance with complicated geometry triangular elements were used in the 2D model and hexahedral elements with linear approximation in the 3D model. The mesh generation had to be paid close attention, i.a. because the triangular elements or hexahedrons which degenerated in wedges exhibit nonsymmetric response to symmetrical load, which leads to so-called *shear locking*. To avoid this phenomenon it was necessary to edit the 2D model was necessary to edit very carefully by hand.

Calculations using SIFEL package were performed for the selected three segments of massif. In this case the mechanical part of the program, called MEFEL, was used and nonlinear behavior of material was modelled using Mohr-Coulomb plasticity. Material characteristics for this model were available. This model seemed to be optimal and for rock simulation and for obtaining the critical load coefficient, at which the failure of rock takes place. As the nonlinear equation system was solved by the Newton-Raphson method, the iterative process was controlled by load increment. With regard to the high number of equations and the high number of nonzero elements in system matrix the so-called *sparse direct solver* was used to solve the equation system, which dramatically reduced time requirements (up to 10 times as compared with the standard LDL decomposition method). For illustration the number of nodes and elements, the number of equations and the number of nonzero elements in the system matrix for support No. 10 are given in Tab. (4.2).

Number of 3D elements	32460
Number of nodes	18678
Number of unknowns	50962
Number of nonzero elements of matrix	34038279

Table 4.2: Computation demand factor for model segment at pier No. 10

During computations one paradox appeared. Experience has shown that it is better to use the initial material stiffness matrix than the tangent one, because in case of the tangent matrix it is necessary to assemble the system matrix and solve the equation system in every iteration step. On the other hand, in case of initial stiffness matrix it is possible store the decomposed system matrix and to perform only backward substitution

during the iteration steps. The disadvantage of this approach is that it increases the volume of iteration steps; in this case, however, greater iteration extent was preferable to the solution of the system of equations. For every segment model of the massif calculation of two combinations of load cases were made :

1. The model was loaded only with dead weight of the massif, load factor was increased to value $\lambda_f = 1.1$.

2. The model was loaded with :

   - dead weight of the massif and the bridge - load factor was increased to value $\lambda_f = 1.1$
   - pressure at rest of the rock massif - load factor was increased to value $\lambda_f = 1.0$
   - life load - load factor was increased to value $\lambda_f = 1.4$ or on to collapse value

The values of the material parameter were taken as standard ($\gamma_m = 1.0$). The whole calculation of one support segment under the above mentioned conditions on a computer with AMD Athlon 2800+ processor with 512 MB memory took about 2 hours.
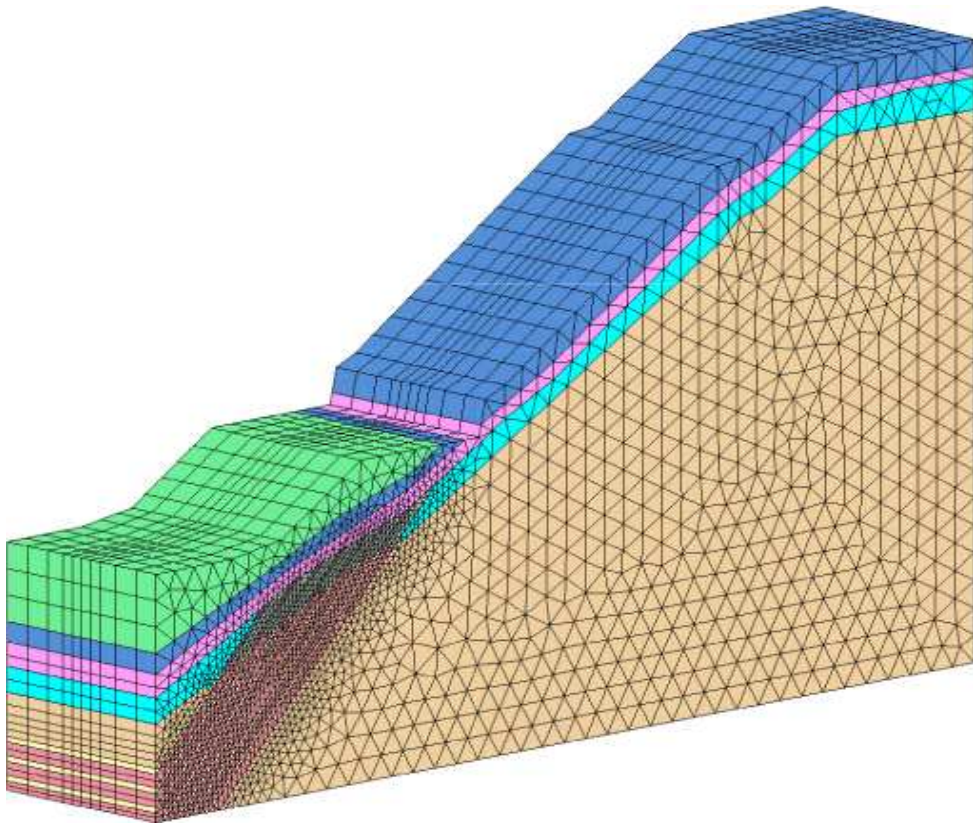
Figure 4.8: 3D mesh of finite elements for the segment of pier No. 4
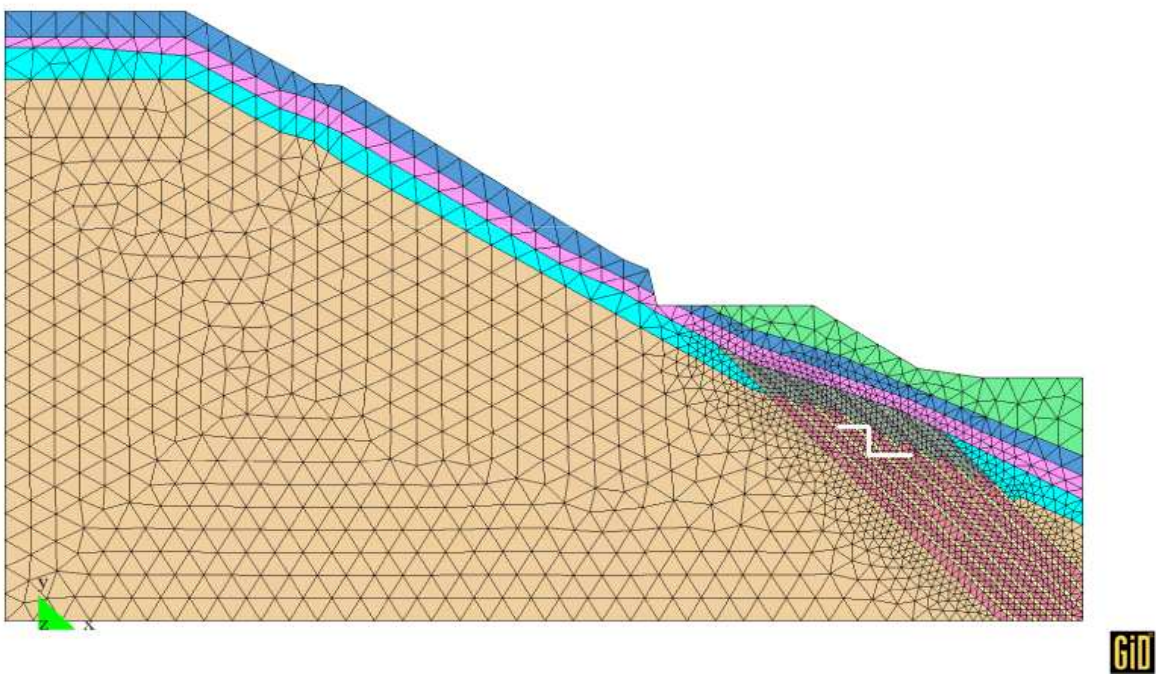
Figure 4.9: 2D mesh of finite elements for the segment of pier No. 4 with plotted footing base
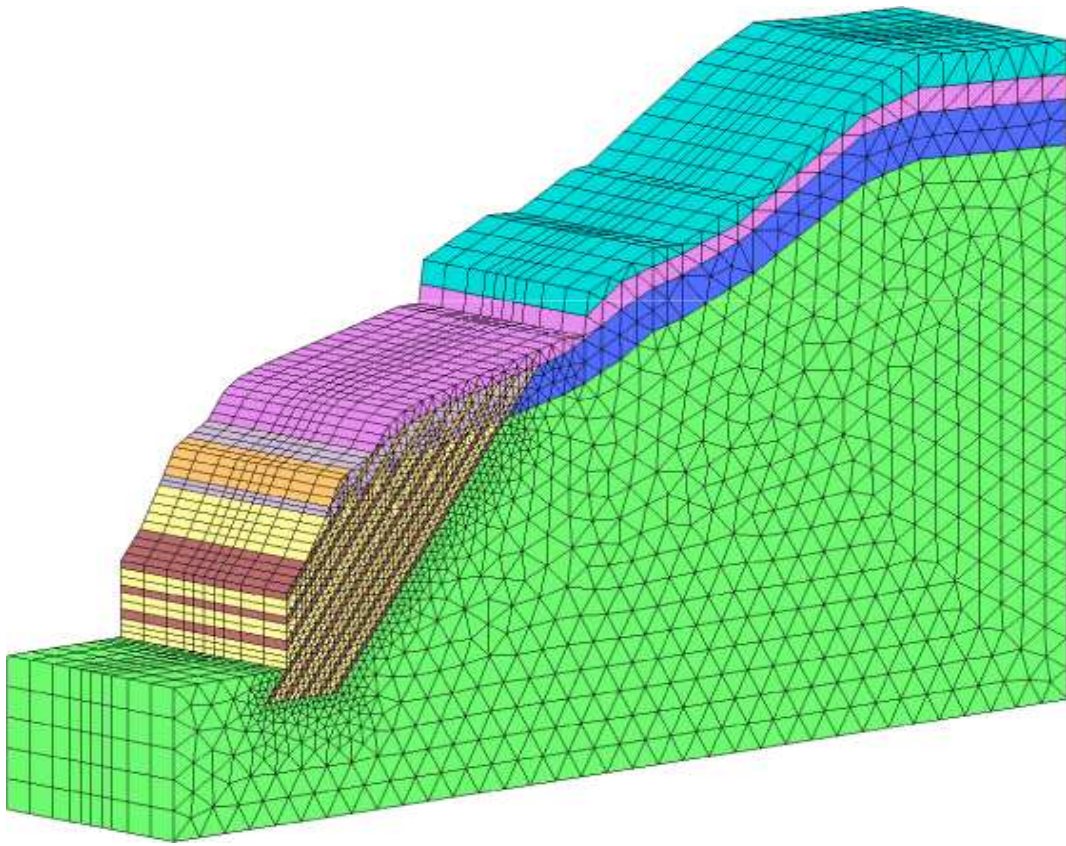
Figure 4.10: 3D mesh of finite elements for the segments of piers No. 10
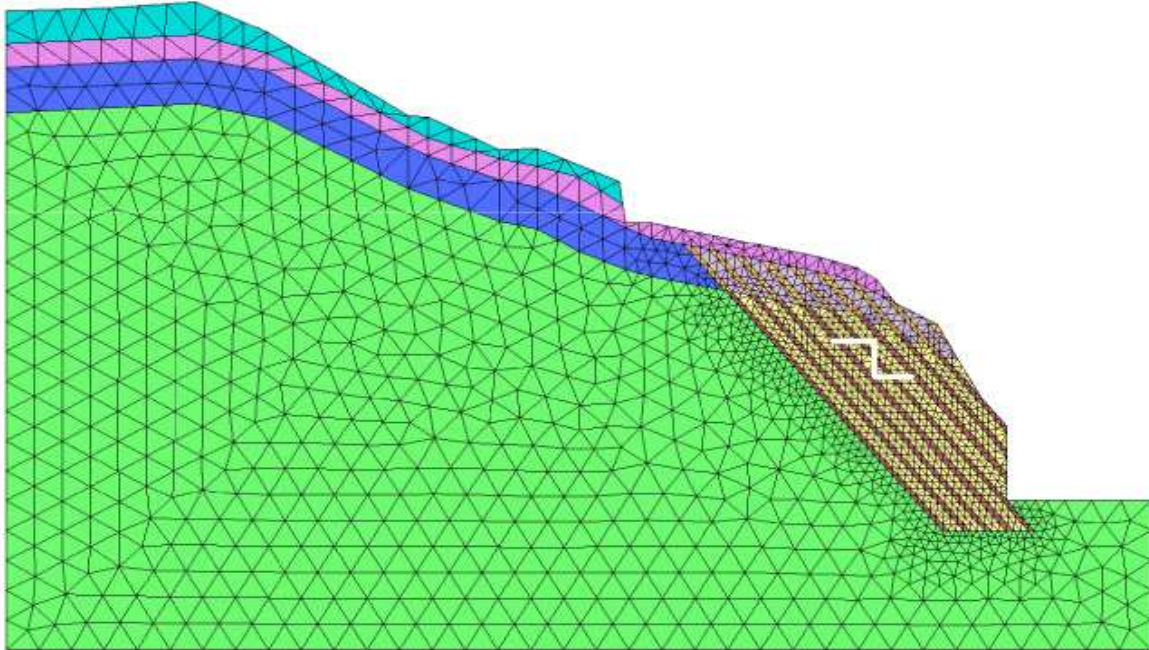
Figure 4.11: 2D mesh of finite elements for the segment of pier No. 10 with plotted footing base
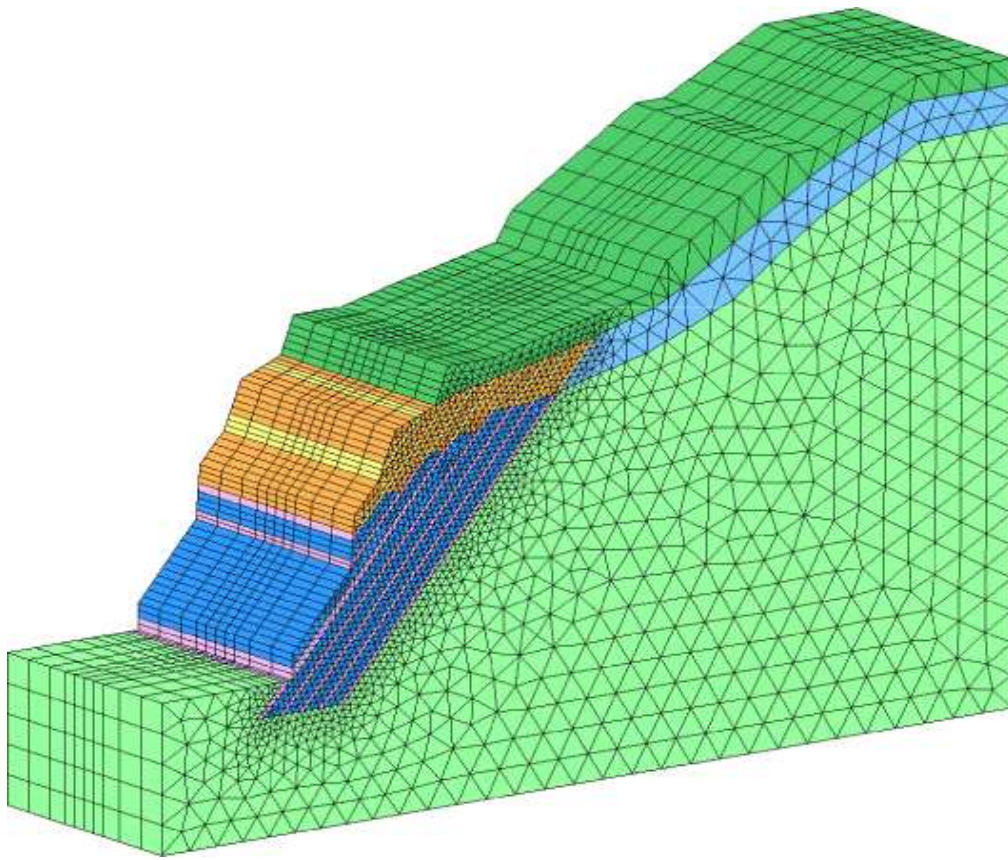
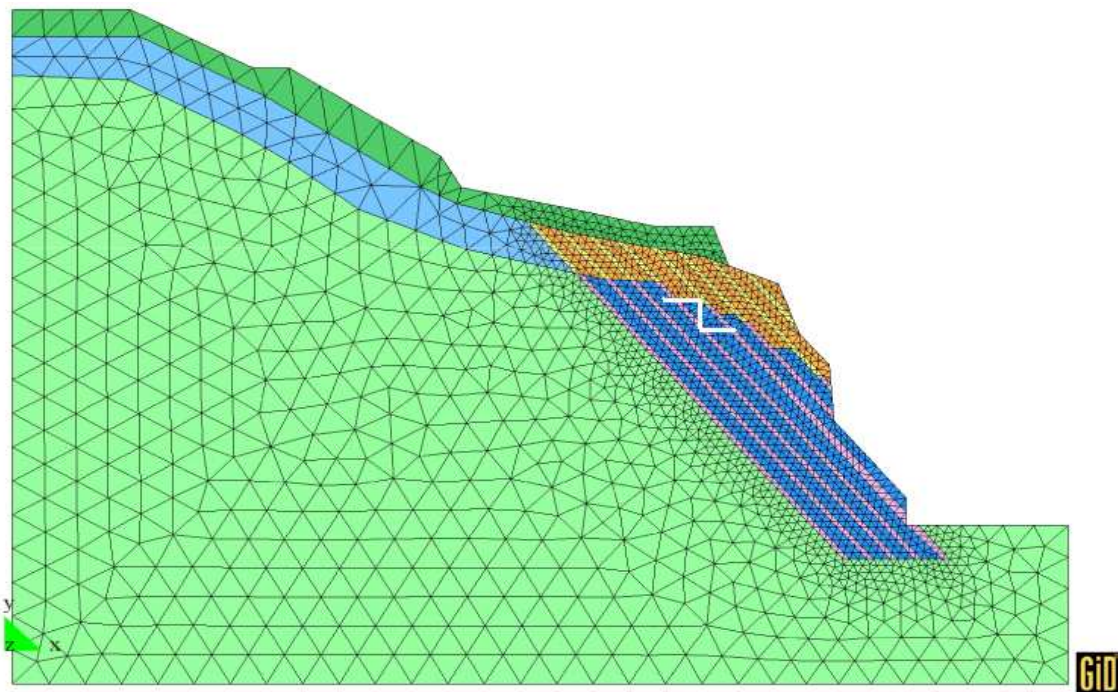Figure 4.12: 3D mesh of finite elements for the segments of piers 12

Figure 4.13: 2D mesh of finite elements for the segments of piers 12 with plotted footing base

76

4.5   Results and Conclusions

Objectives of analyses were to determine the load factor at which the plasticity is reached and the slip surface originates. From these viewpoints the most critical situation is near piers No. 10 and No. 12 . The neighborhood of pier No. 4 exhibits plastic flow only in embankment surface strata and at the footing base, which, however, does not affect the overall stability of the rock massif.

Analysis of segment No. 10 for both limiting combinations of load cases showed only one and very critical zone, with an already existing critical plasticized slip surface (see Figs. (4.16) and (4.16)). The surface is generated by plasticized inlay slate outgoing from toe off-cut for excavation of Hoffihotel building and through the front half of the lower footing base and its slope is virtually coincident with the stratification slant of the massif. This surface have been already formed at load factor $\lambda_f < 0.8$. Raising load coefficient for accidental load didn't have any effect on the evolution of the surface,causing only the local plastic zone in footing base surroundings to extend.

In the neighborhood of pier 12 the occurrence of 3 plastic zones was discovered, namely at the of footing base, further around the toe of the intermediate off-cut in the slope below the bridge and in the surroundings of the slope toe. The first two are the rock mass response to the load at both footing base levels and to the weight of surface strata, which lose footholds by spurning approximately in the midst of slope below the bridge. In last named zone the rock mass responds to the pressure of all undercut strata. The massif began to change linear behavior into nonlinear after the load factor $\lambda_f = 0.86$ had been reached. In all cases the course of the stresses exhibited concentration in quartzite inlays (see Figs. (4.19), (4.20) and (4.21)).

Further calculations showed, that segment 4 embodies sufficient stability and only surface strata below the road can show the tendency to creep.

Endangered place with the biggest hazards is the space above the Hoffihotel. Analyses showed that in the segments in the neighborhood of piers No. 10 and 12, the stability of the model even for dead weight load for the given standard values approaches to the critical value of Fs = 1 and can be ever lower. The currently morphologically stable behavior can be only temporary. Long-term measurements show continual moves in order of mm. As a part of these movements is caused by the movement along a laminated surface, these surfaces are successively polished and the shear strength diminishes to residual values.

Generally it is possible to say, that the rock mass under the elevated road is probably in an indifferent equlibrium near critical stability and that this equilibrium depends on the state of plasticized zones of the rock massif. The massif stability under the examined piers No. 10 and 12 has not required the standard values. Live load from transport does not play a dominant role, but it could play an activating role.

In addition to the final technical report to the client, the results were presented at conferences and published in [24], [29] and [30].

4.6   Resulting Pictures of Selected Quantities

This section contains pictures produced during the calculations. Only the most important pictures were selected from the quite big amount of output data. As the neighborhood of pier No. 10 can be considered as the most dangerous among the analyzed areas, most

illustrations concern this case. The resulting pictures from the remaining two analyses are also available, but only plastic zones were selected. If the figures contain plastic zones, the contour surfaces of the total value of consistency parameter were plotted. In case of stresses the values are in [Pa] units.
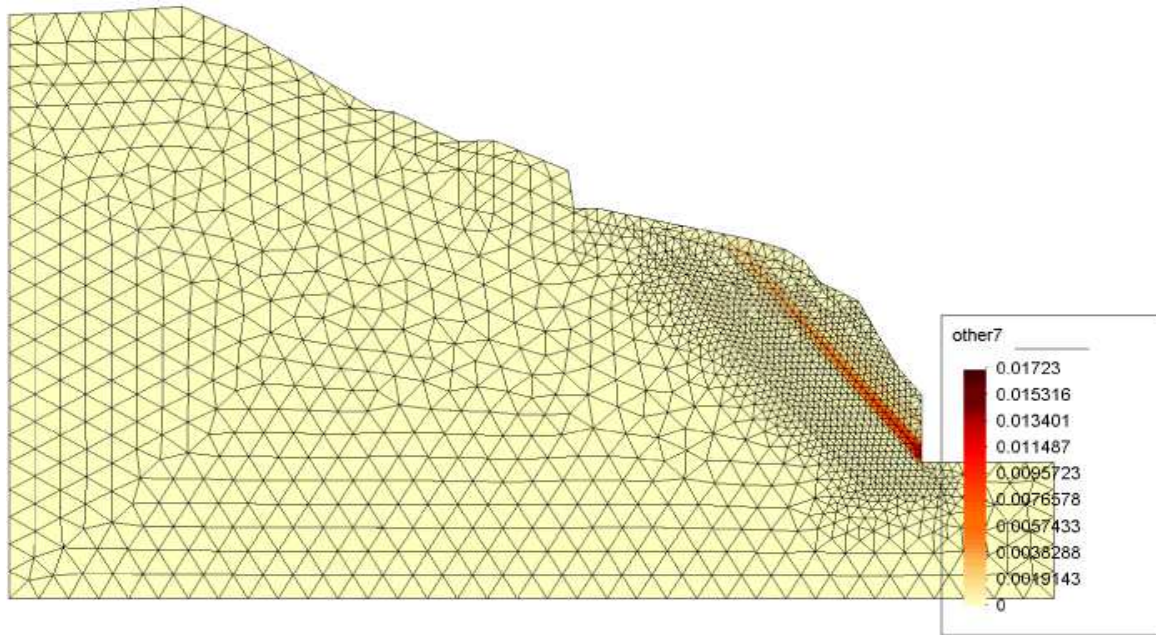
Figure 4.14: Segment of pier No. 10 (load combination 1, reached load factor $\lambda_f = 1.1$) : Plastic zones - values of consistency parameter
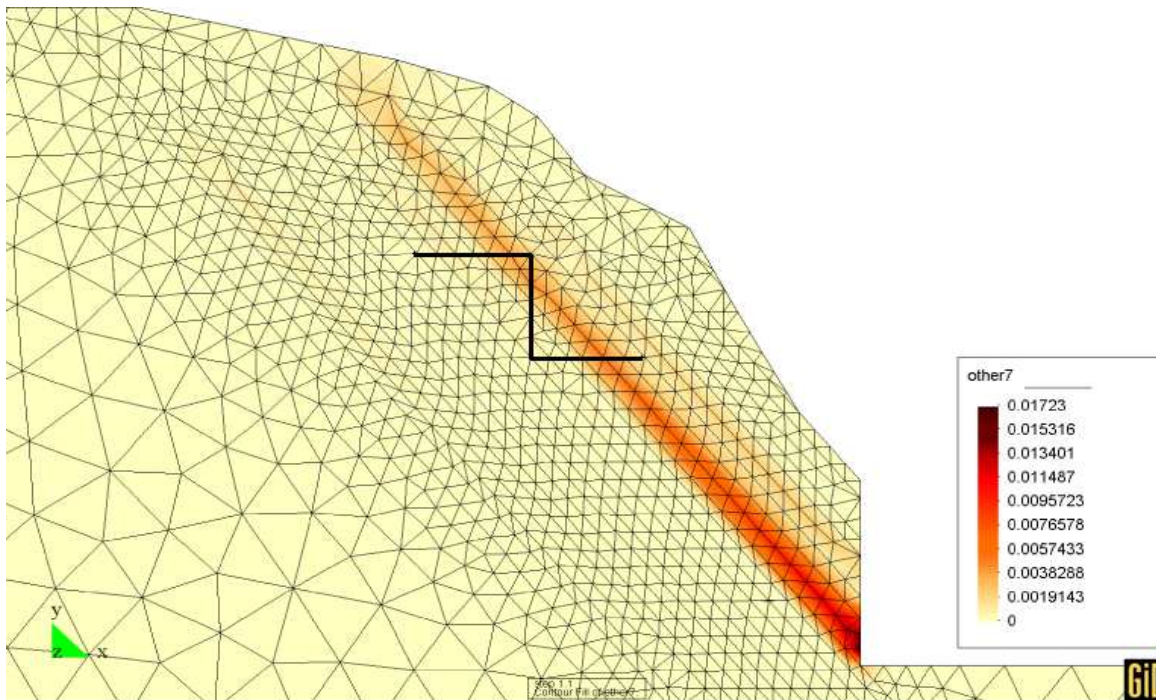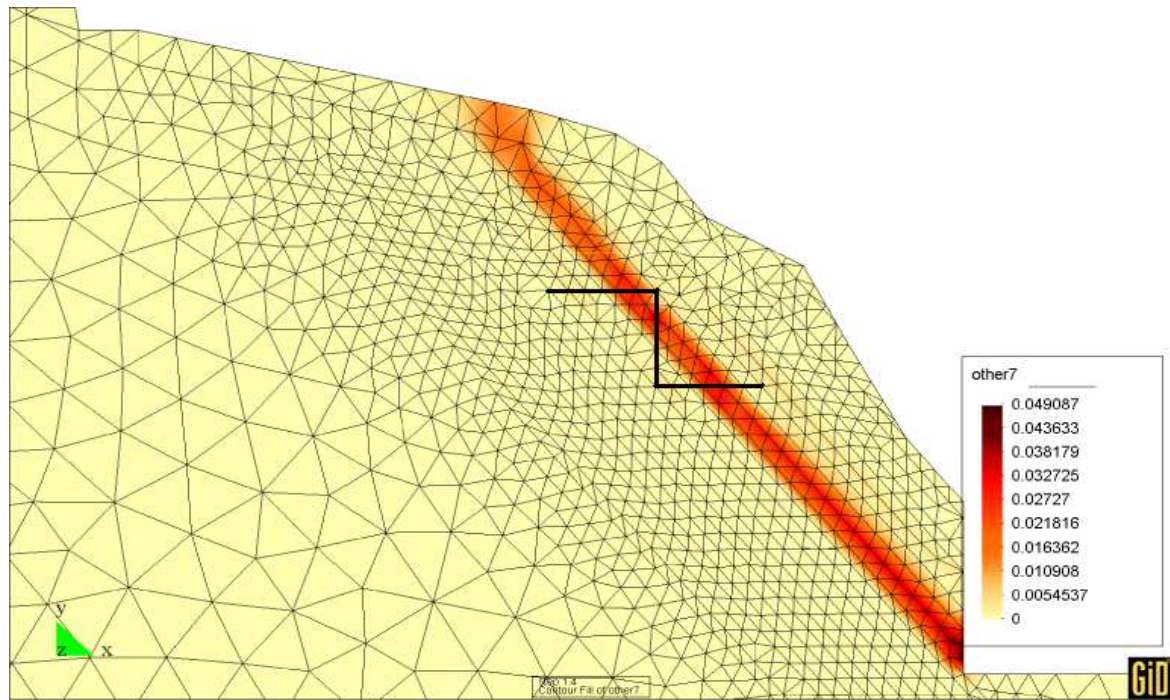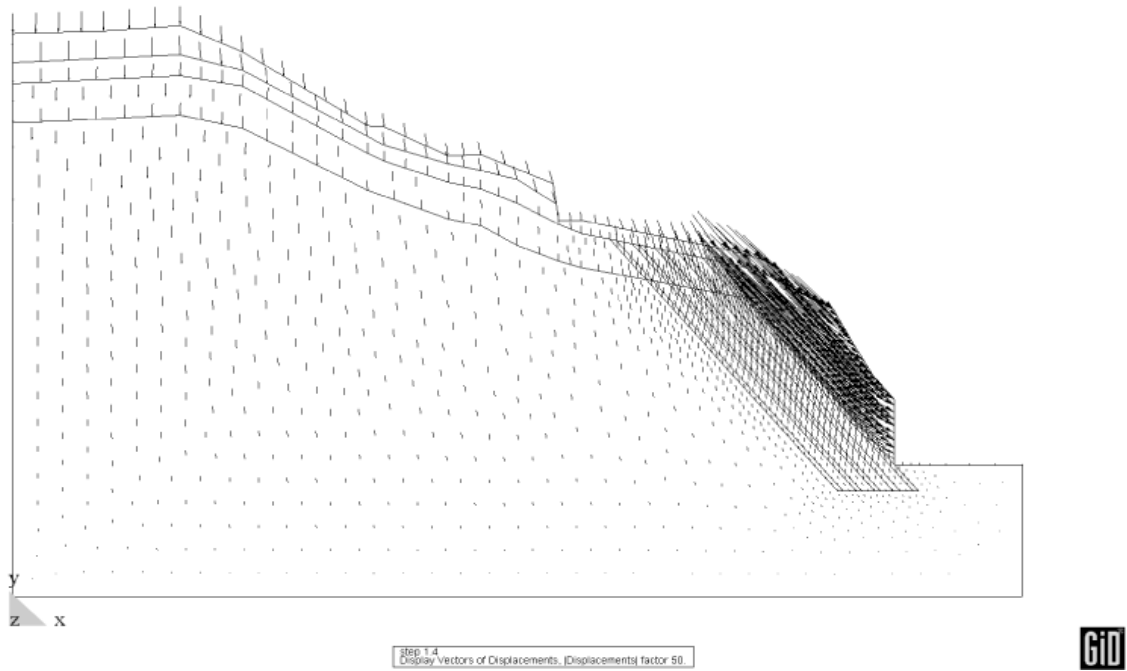

Figure 4.15: Segment of pier No. 10 (load combination 1, reached load factor $\lambda_f = 1.1$) : Detail of plastic zones - values of consistency parameter
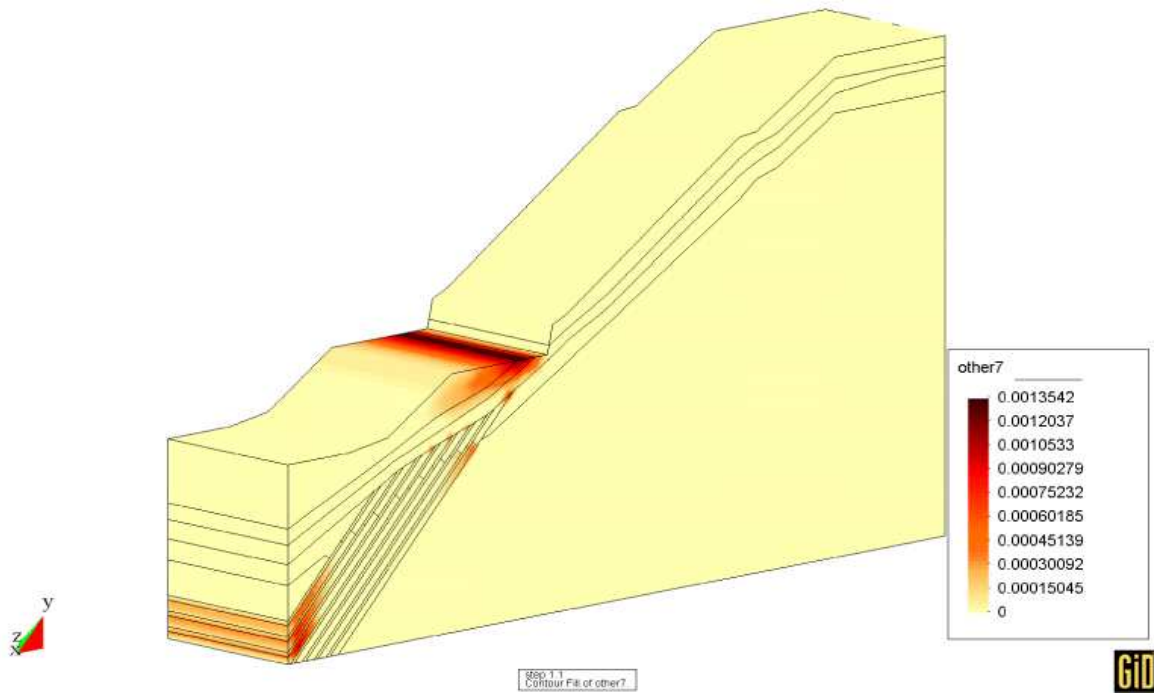
79

Figure 4.16: Segment of pier No. 10 (load combination 2, reached load factor $\lambda_f = 1.4$) : Plastic zones - values of consistency parameter
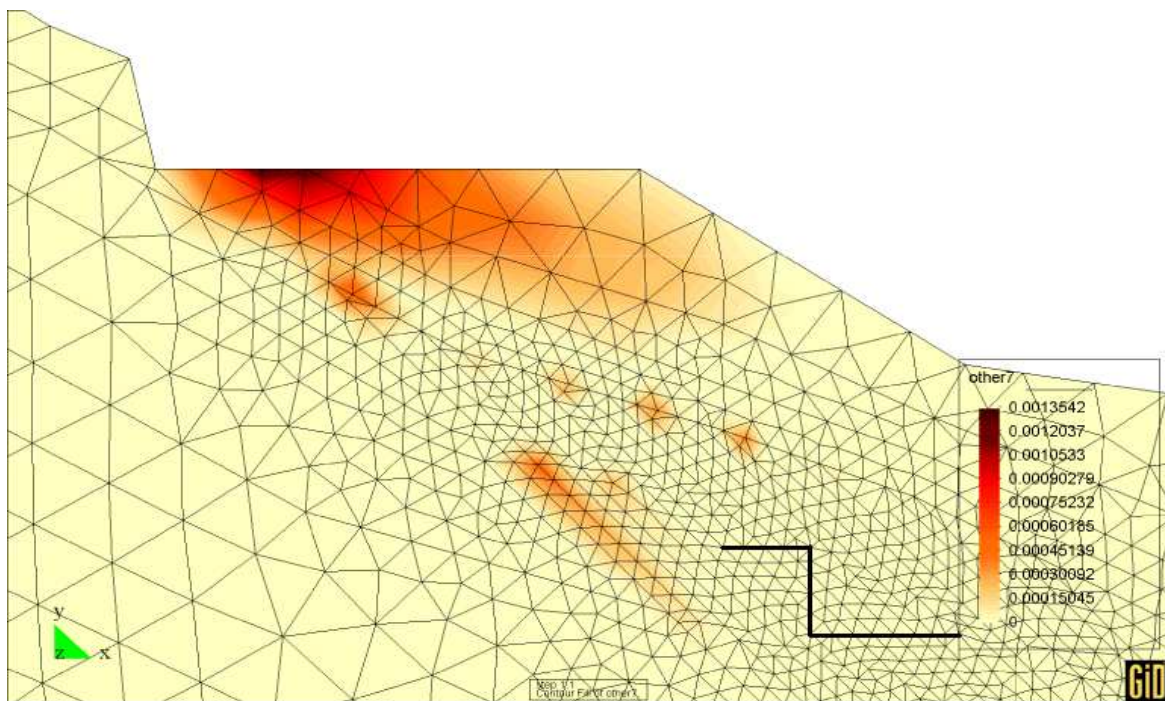

Figure 4.17: Segment of pier No. 10 (load combination 2, reached load factor $\lambda_f = 1.4$) : Detail of plastic zones - values of consistency parameter

Figure 4.18: Segment of pier No. 10 (load combination 2, reached load factor $\lambda_f = 1.4$) : Directions of total displacements
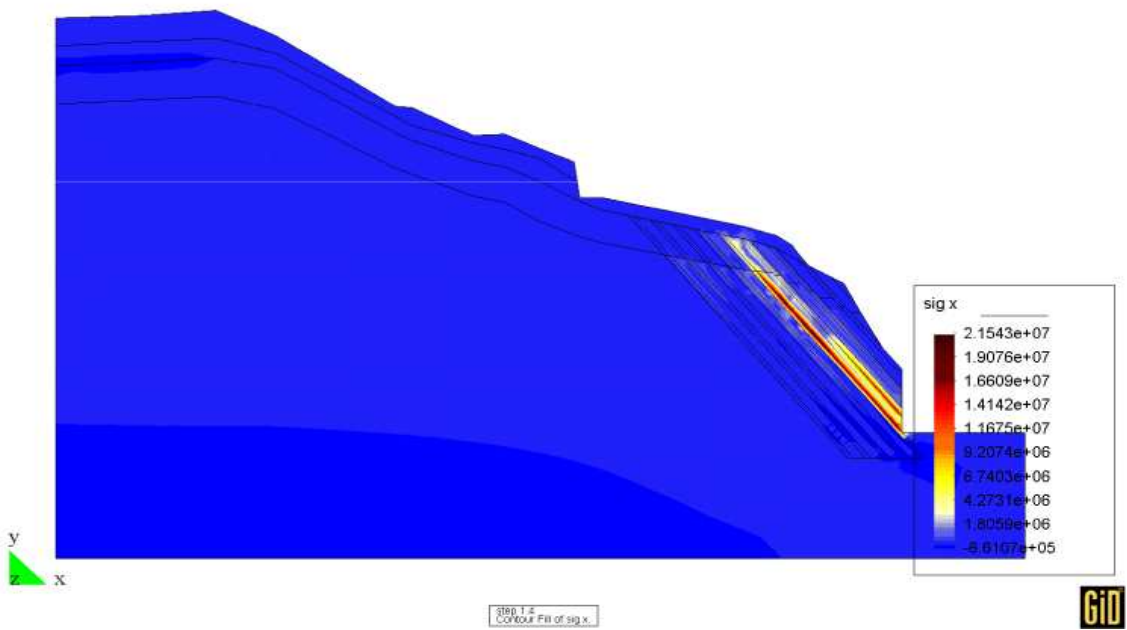
Figure 4.19: Segment of pier No. 10 (load combination 2, reached load factor $\lambda_f = 1.4$) : Horizontal stresses σ_x
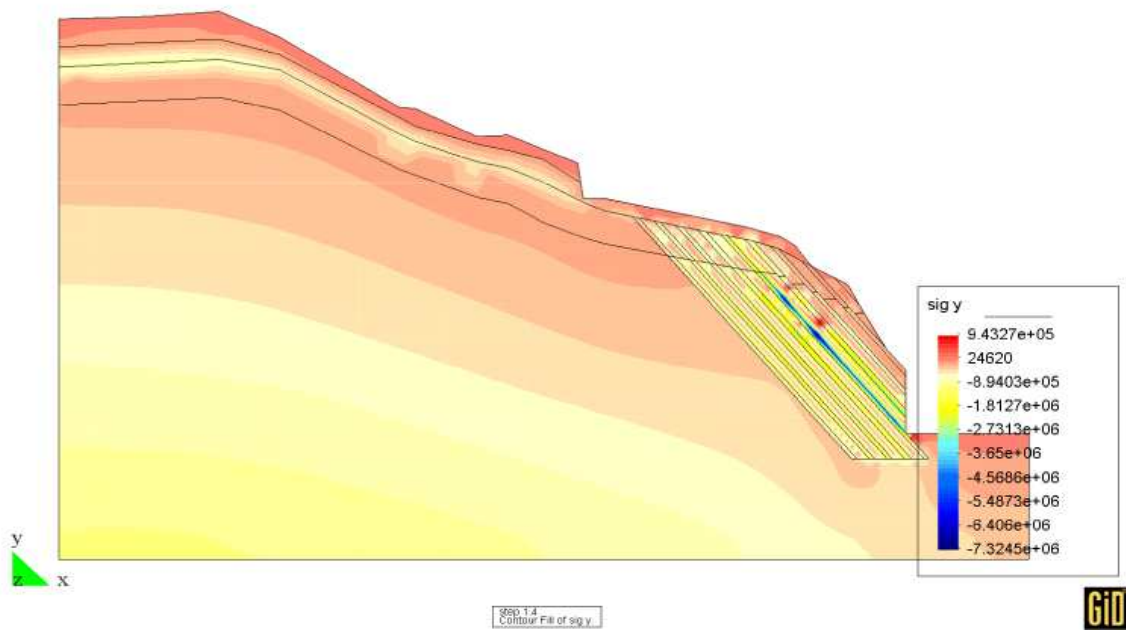
Figure 4.20: Segment of pier No. 10 (load combination 2, reached load factor $\lambda_f = 1.4$) : Vertical stresses σ_x
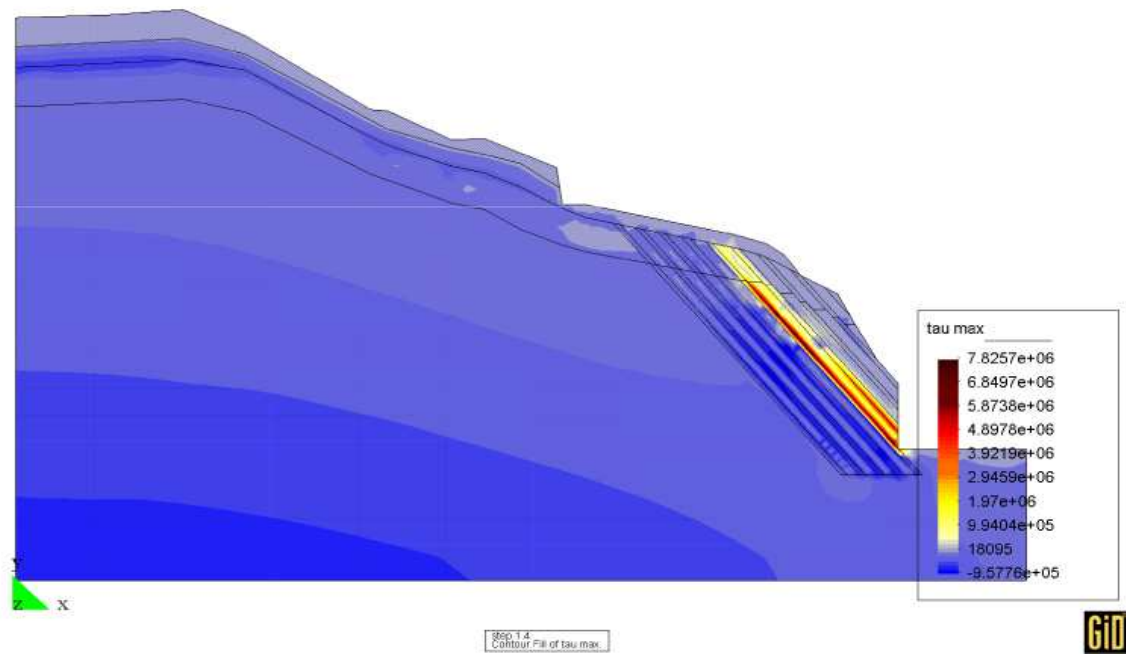
Figure 4.21: Segment of pier No. 10 (load combination 2, reached load factor $\lambda_f = 1.4$) : Principal shear stresses τ_{max}
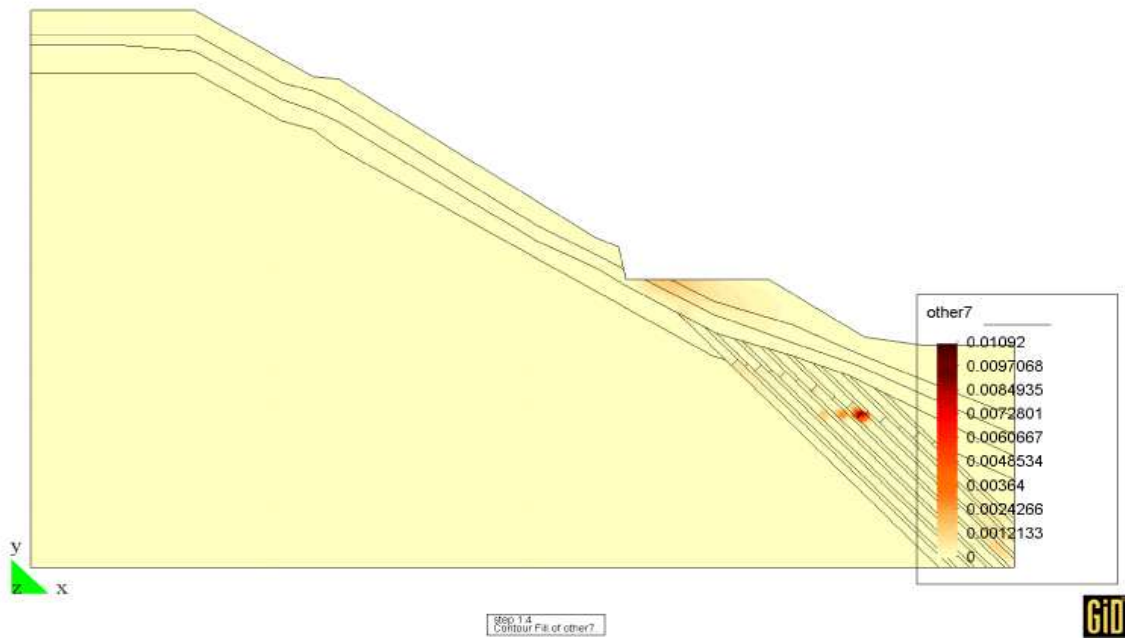
Figure 4.22: Segment of pier No. 4 (load combination 1, reached load factor $\lambda_f = 1.1$) : Plastic zones - values of consistency parameter
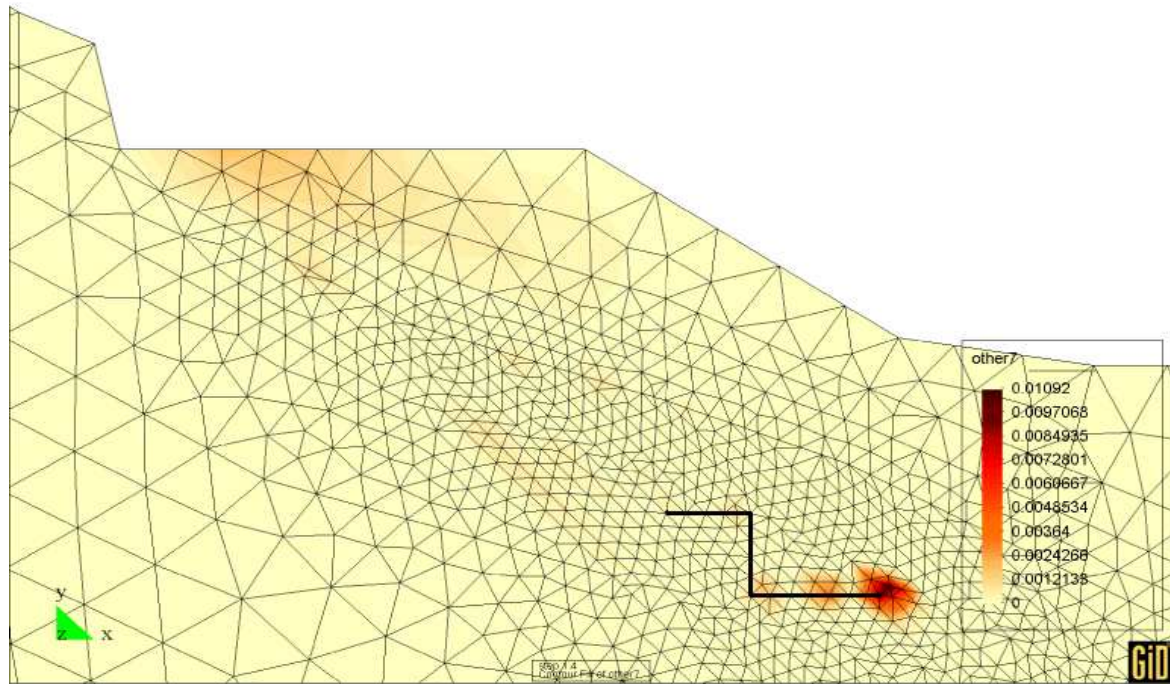

Figure 4.23: Segment of pier No. 4 (load combination 1, reached load factor $\lambda_f = 1.1$) : Detail of plastic zones - values of consistency parameter
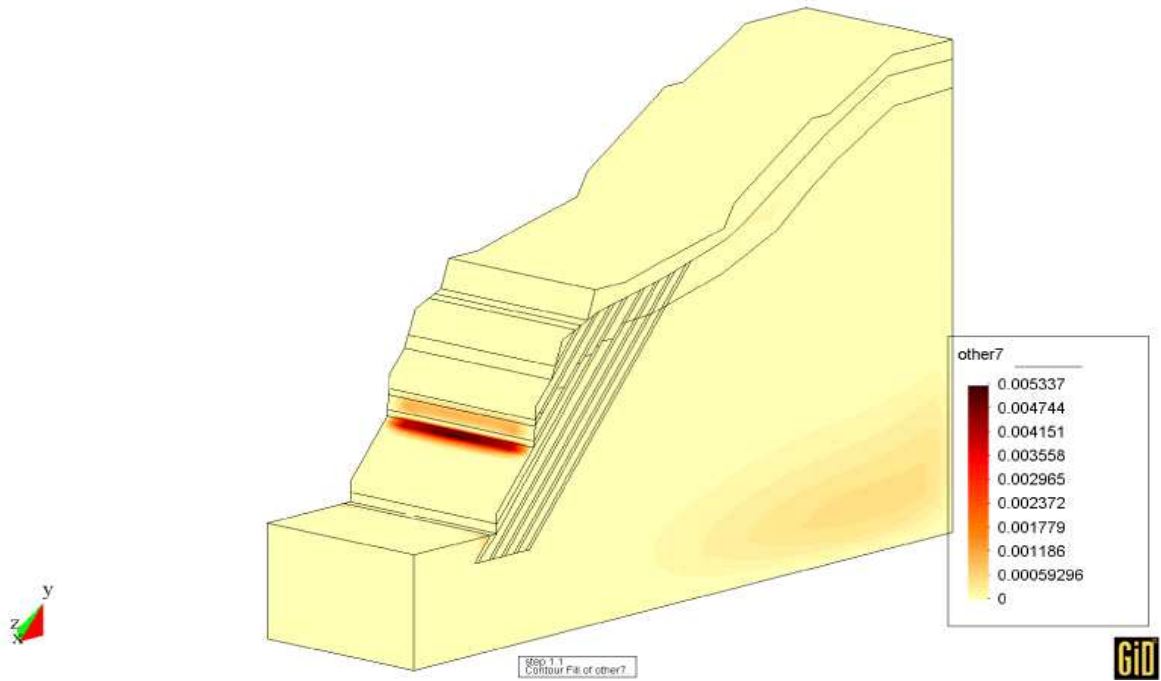
83

Figure 4.24: Segment of pier No. 4 (load combination 2, reached load factor $\lambda_f = 1.4$) : Plastic zones - values of consistency parameter
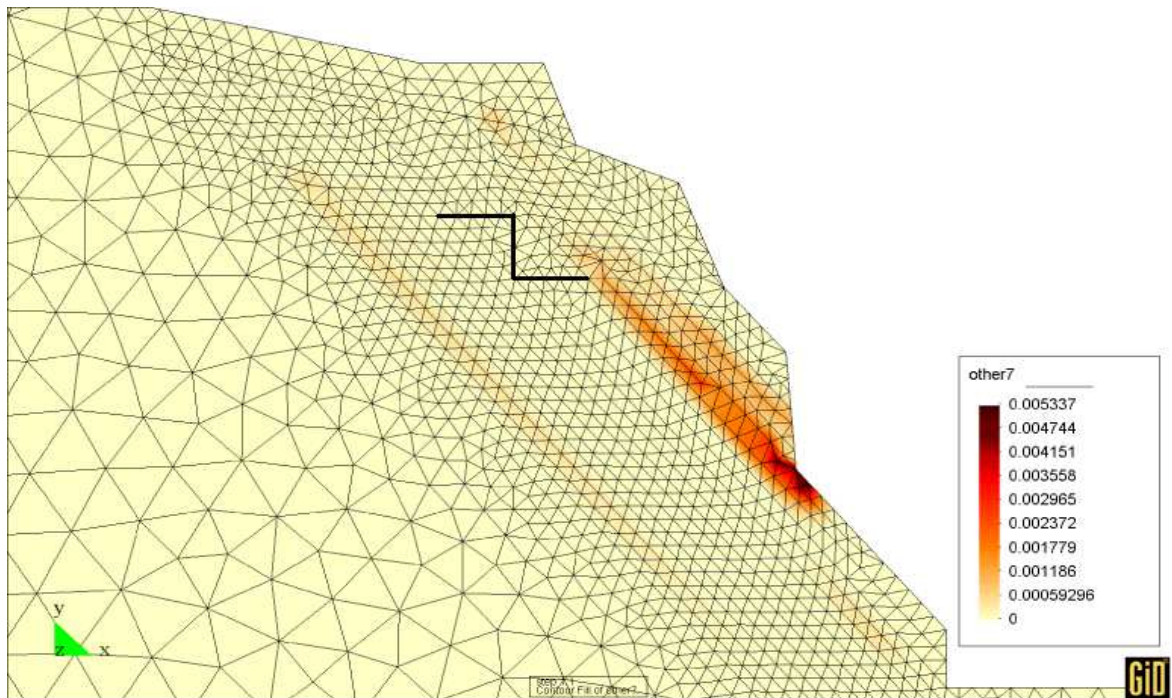

Figure 4.25: Segment of pier No. 4 (load combination 2, reached load factor $\lambda_f = 1.4$) : Detail of plastic zones - values of consistency parameter

84

Figure 4.26: Segment of pier No. 12 (load combination 1, reached load factor $\lambda_f = 1.1$) : Plastic zones - values of consistency parameter

Figure 4.27: Segment of pier No. 12 (load combination 1, reached load factor $\lambda_f = 1.1$) : Detail of plastic zones - values of consistency parameter
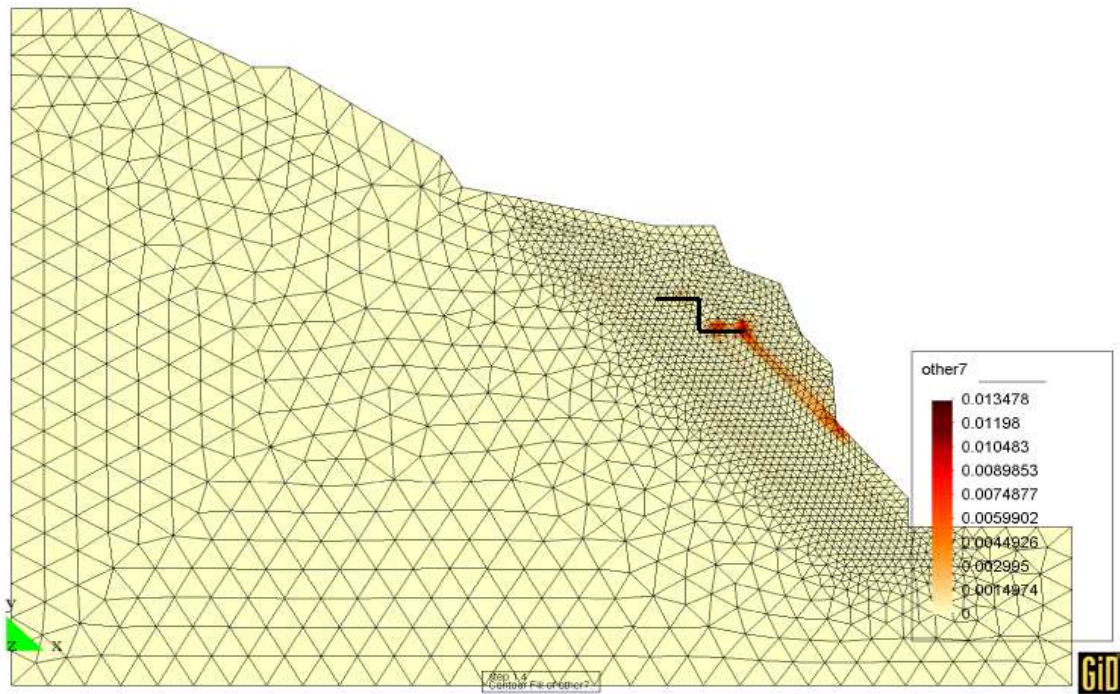
Figure 4.28: Segment of pier No. 12 (load combination 2, reached load factor $\lambda_f = 1.4$) : Plastic zones - values of consistency parameter
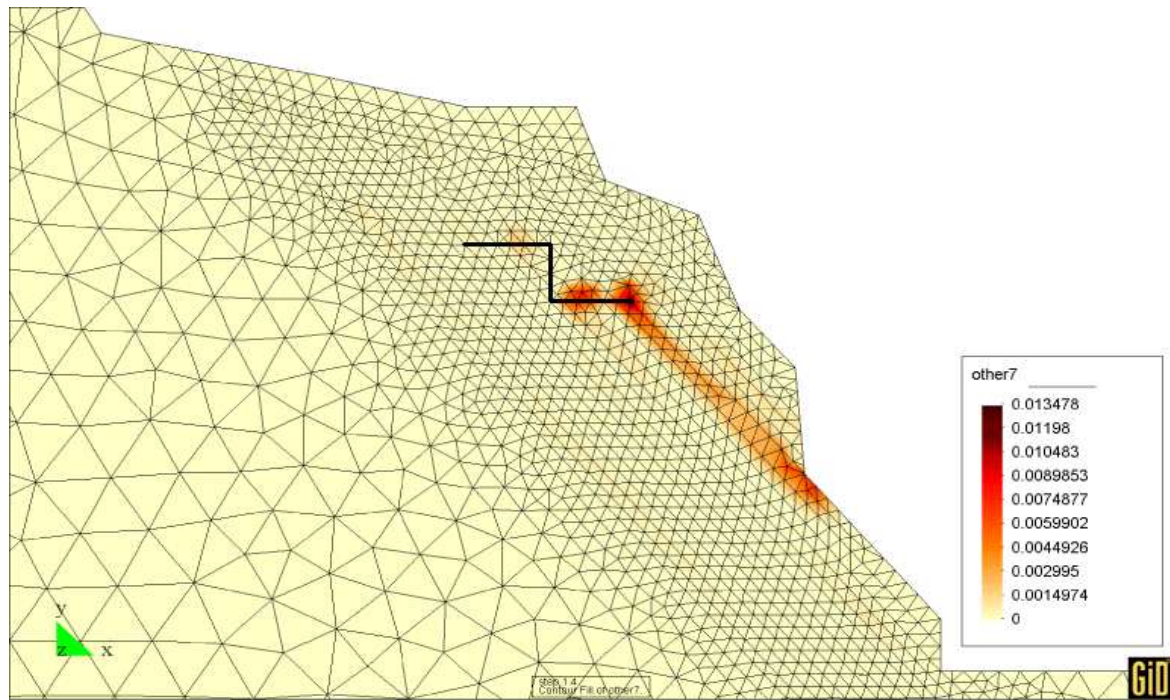

Figure 4.29: Segment of pier No. 12 (load combination 2, reached load factor $\lambda_f = 1.4$) : Detail of plastic zones - values of consistency parameter

86